Agglomeration Drives the Reversed Fractionation of Aqueous Carbonate and Bicarbonate at the Air-Water Interface

Shane W. Devlin[1,2,§], Sasawat Jamnuch[3,§], Amanda A. Chen[3], Qiang Xu[2], , Jin Qian*[2]

Tod A. Pascal*[3,4,5] and Richard J. Saykally*[1,2]

§: These authors contributed equally to this work.

1: Department of Chemistry, University of California, Berkeley, CA 94720, USA.

2: Chemical Sciences Division, Lawrence Berkeley National Lab, Berkeley, CA 94720, USA.

3: ATLAS Materials Science Laboratory, Department of Nano Engineering and Chemical Engineering, University of California, San Diego, La Jolla, California, 92023, USA.

4: Materials Science and Engineering, University of California San Diego, La Jolla, California, 92023, USA.

5: Sustainable Power and Energy Center, University of California San Diego, La Jolla, California, 92023, USA.

*: Corresponding Authors: Richard J. Saykally: saykally@berkeley.edu;

Tod A. Pascal: tpascal@ucsd.edu; Jin Qian: jqian2@lbl.gov

Table of Contents

A. Experimental Methods and Materials

A.1. Materials: All glassware was soaked overnight in Alnochromix (Alconox Inc.) cleaning solution and rinsed thoroughly with ultrapure (18.2 MΩ) water. Solutions were prepared by dissolving reagent grade sodium carbonate (Sigma Aldrich, >99% purity) and sodium bicarbonate (Sigma Aldrich, >99% purity) in ultrapure water.

A.2. Second Harmonic Generation Spectroscopy: The experimental design has been described in detail elsewhere[1], and only a brief description is given here. The output from a Ti-S regenerative amplifier (Spectra Physics Spitfire, 4 mJ, 100fs, 1kHz) is directed through a BBO crystal to generate light at 400 nm. The 400 nm light is then focused onto the surface of the solution using a $f =$ 100mm lens at an angle of 60° relative to the surface normal. The fundamental and SH light are collected with a collimating lens, and the fundamental light is spectrally filtered using a laser line mirror and Pellin-Broca prism. The SH photons are then detected using a gated boxcar integrator (Stanford Research Systems), a monochromator (Acton SpectraPro 2150i), and a photomultiplier (Hamamatsu, R7154PHA) for photon counting. All SHG measurements are normalized relative to the SH response of pure water. Input polarization was controlled using a half-wave plate and a polarizer.

A.3. Derivation of Langmuir Adsorption Model for Use in SHG: The second harmonic (SH) intensity can be written as:

$$I_{SH} \propto \left|\chi^{(2)}\right|^2 I_\omega^2 \qquad (1)$$

Here $\chi^{(2)}$ is the second-order susceptibility and I_ω is the intensity of the fundamental light. $\chi^{(2)}$ is complex valued, and has a contribution from each component in the system:

$$\frac{I_{SH}}{I_\omega^2} \propto \left|\chi^{(2)}_{water} + \chi^{(2)}_{anion}\right|^2 \qquad (2)$$

$\chi^{(2)}$ is dependent on the number density, *N*, as well as the effective hyperpolarizability, β^{eff}:

$$\frac{I_{SH}}{I_{\omega}^2} \propto \left| N_{water} \times \beta_{water}^{eff} + N_{anion} \times \beta_{anion}^{eff} \right|^2 \qquad (3)$$

Water does not give a strong SH response, and we assume its contribution to the signal is real. However, because carbonate and bicarbonate are resonant at the SH wavelength, they have both real and imaginary components. We can group these contributions according to

$$\frac{I_{SH}}{I_{\omega}^2} \propto \left(N_{water} \times \beta_{water}^{eff} + N_{anion} \times \mathrm{Re}\left\{ \beta_{anion}^{eff} \right\} \right)^2 + \left(N_{anion} \times \mathrm{Im}\left\{ \beta_{anion}^{eff} \right\} \right)^2 \qquad (4)$$

and switch to using relative surface population by dividing each term by N_{water}:

$$\frac{I_{SH}}{I_{\omega}^2} \propto \left(\beta_{water}^{eff} + \frac{N_{anion}}{N_{water}} \times \mathrm{Re}\left\{ \beta_{anion}^{eff} \right\} \right)^2 + \left(\frac{N_{anion}}{N_{water}} \times \mathrm{Im}\left\{ \beta_{anion}^{eff} \right\} \right)^2 \qquad (5)$$

which simplifies to:

$$\frac{I_{SH}}{I_{\omega}^2} \propto \left(A + N_s \times B \right)^2 + \left(N_s \times C \right)^2 \qquad (6)$$

Here, the weak system response from water is represented by the non-resonant term *A*, *B* is the real component of the anion susceptibility, *C* is the imaginary component of the anion susceptibility, and N_s is the surface population (sometimes referred to as fractional coverage) of surface-active anions.

To develop an expression for the number of surface-active anions, N_s, we use the Langmuir adsorption model, where an anion in the bulk can exchange with a water at the surface:

$$Anion_{bulk} + water_{surf} \leftrightarrow Anion_{surf} + water_{bulk} \qquad (7)$$

Here, the subscripts *surf* and *bulk* refer to an anion/water molecule occupying a surface site or bulk site, respectively. We can write the equilibrium expression according to the concentration of each species as:

$$K_{ads} = \frac{[Anion]_{surf} \times [water]_{bulk}}{[Anion]_{bulk} \times [water]_{surf}} \qquad (8)$$

If we assume a maximum number of surface sites, $[sites]_{max}$ the expression becomes:

$$K_{ads} = \frac{[Anion]_{surf} \times [water]_{bulk}}{[Anion]_{bulk} \times \left([sites]_{\max} - [Anion]_{surf}\right)} \qquad (9)$$

Here, we are assuming a surface site can only be occupied by one adsorbate.

Rearranging for $[Anion]_{surf}$ gives:

$$N_s = [Anion]_{surf} = [sites]_{\max} \times \frac{[Anion]_{bulk}}{[water]_{bulk} \times K_{ads}^{-1} + [Anion]_{bulk}} \qquad (10)$$

Substituting N_s back into Equation (6), gives:

$$\frac{I_{SH}}{I_{\omega}^2} \propto \left(A + B \frac{[Anion]_{bulk}}{[water]_{bulk} \times K_{ads}^{-1} + [Anion]_{bulk}} \right)^2 + \left(C \frac{[Anion]_{bulk}}{[water]_{bulk} \times K_{ads}^{-1} + [Anion]_{bulk}} \right)^2 \qquad (11)$$

where $[sites]_{max}$ has been absorbed into the fitting parameters B and C. We then divide both the top and bottom by ($[Anion]_{bulk}$ + $[water]_{bulk}$) to change to mole fraction and lastly use the relationship between the equilibrium adsorption rate and the Gibbs free energy:

$$K_{ads} = e^{-\Delta G/RT} \qquad (12)$$

to yield the final fitting equation:

$$\frac{I_{SH}}{I_{\omega}^2} \propto \left(A + B \frac{X_{anion}}{(1 - X_{anion}) e^{\frac{\Delta G}{RT}} + X_{anion}} \right)^2 + \left(C \frac{X_{anion}}{(1 - X_{anion}) e^{\frac{\Delta G}{RT}} + X_{anion}} \right)^2 \qquad (13)$$

which relates the observed SH intensity to the bulk anion mole fraction (X_{anion}) and the Gibbs free energy of adsorption (ΔG).

B. Computational Methods

B.1. Carbonate forcefield and new species parameterization: We are interested in the assessing the propensity for carbonates/bicarbonate/carbonic acid/carbon dioxide species, as isolated species and agglomerates, in the bulk and at the interface, while studying systems of length scales approaching the experimental micromolar

concentrations. These requirements place strict restrictions on the level of theory that can be employed: the systems are generally too large for practical calculations using approaches where the energy is obtained from Quantum Mechanical (QM) electronic structure calculations, however the physics of the varied electrostatic environment needs to be accounted for. It has been recognized recently[2-4] that models that explicitly account for atomic/molecular polarization physics are required. In this work we adopt an approach where all the species are described using the AMOEBA forcefield, where the particular parameter set been validated to reproduce the experimental lattice and parameters of the solid (calcite), while also accurately predicting the hydration free energy of carbonate/bicarbonate.[2, 4] The details of the AMOEBA class of potentials have been detailed elsewhere,[5] but in short, it is a polarizable forcefield with explicit terms describing electrostatic interactions between permanent point charges, dipoles and quadrupoles. In the present case, we augment the carbonate-AMOEBA forcefield of Gale and coworkers with parameters for the sodium ion parameters from the AMOEBA-04[5] parameter set, while parameters for carbonic acid and carbon dioxide were generated using the Poltype2[6] automatic parameter generation engine. The water molecules were described using the AMOEBA-water-03 forcefield. We validate that our parameters were adequate by calculating the hydration free energies using free energy perturbation (FEP) of carbonate/bicarbonate/carbon dioxide (see discussion below), as well as the density and cohesive energy of Natrite, all of which were found to be in good agreement with experiments and previously published results (**Table S3**). In the case of carbonic acid, there is no adequate experimental solvation free energy to compare to, so we performed quantum chemistry calculations at the B3LYP/aug-cc-pvtz level of theory, using the SM8 solvation model[7] in Q-Chem 6.0 electronic structure package,[8] which showed very good agreement with our MD FEP results. The full parameter set used in this study is included as a supporting data file.

B.2. MD simulation Equilibration Procedure: All simulations were performed using the LAMMPS MD engine.[9] We equilibrated each system by our usual equilibration procedure:[10-22] first, we performed an initial energy minimization at 0 K (energy and force tolerances of 10^{-4}) using the conjugate gradient minimization scheme to obtain the ground-state structure. Then, the system was slowly heated from 0 K to 298K at constant volume over 0.5 ns using a Langevin thermostat, with a damping parameter of 100 ps. The system was then subjected to 5 cycles of quench-annealing dynamics, with a 500 kcal/mol/Å^2 spring applied to the carbonate species to keep them from moving. Here, the temperature was slowly cycled between 298 K and 894 K over 1 ns using a Nose-Hoover thermostat (temperature relaxation constant of 100 fs), in order to eliminate the persistence of any meta-stable states in the solvent. The equations of motion were integrated by means of the velocity verlet algorithm in a 1 fs timestep. For bulk (3D) simulations, we further equilibrated in the constant temperature (298 K), constant pressure (1bar) (Gibbs or NPT ensemble) for 1 ns. We resolved stresses in the system anistropically using the Andersen barostat (pressure relaxation constant of 1 ps). The equations of motion used are those of Shinoda et al.[23], which combine the hydrostatic equations of Martyna et al.[24] with the strain energy proposed by Parrinello and Rahman.[25] The time integration schemes closely follow the time-reversible measure-preserving Verlet integrators derived by Tuckerman et al.[26] During the last 0.5 ns of the 1 ns NPT simulation, we calculated the average cell lengths and linearly adjusted the final NPT simulation cell to that average over a further 0.1 ns of dynamics. This was followed by a final 1ns of NVT dynamics.

We used the equilibrated bulk system (coordinates and velocities) and input into our slab (2D) simulations. We first inflated the z-dimension of the simulation cell by 10nm and centered the slab within the cell, thus allowing 5ns of vacuum at each surface. In order to confine the molecules within the simulation box in the non-periodic z-direction (a requirement of the LAMMPS code for 2D simulations), the top and bottom of the

simulation box were bounded by a purely repulsive wall, by means of a harmonic potential, $E = K (z - z_0)^2$, truncated at the cutoff distance z_0 = 2Å with a force constant of K = 500 kcal/mol/Å. We also prevented any drift in the z-direction of the water slab by checking and zeroing any momentum in the z-direction every 100ps, using the "fix momentum" functionality in LAMMPS. After initial heating, we performed a 2D-NVT simulation for 4ns. In all cases, the slab was found to be stable over the entire MD simulation, with no significant evaporation observed. During the last 2ns of dynamics, we saved a restart file every 100ps.

B.3. Solvation energy of carbonate species: Free Energy Perturbation (FEP), based on the advancements of Zwanzig[27], is a statistical approach to compute the free energy difference between two states:

$$\Delta G(state_1 \rightarrow state_2) = G(state_2) - G(state_1) = -k_B T \ln \left\langle \exp\left(-\frac{U(state_2) - U(state_1)}{k_B T} \right) \right\rangle \quad (1)$$

where G denotes Gibbs (free) energy, k_B is the Boltzmann constant, and U is internal energy. The solvation energies of the various carbonate species were thus calculated as the sum of multi-stages free energy changes. Here, a coupling parameter λ ($0 \le \lambda \le 1$) is introduced to gradually change the carbonate – water interaction energy, such that the free energy[28] was obtained as:

$$\Delta_0^1 G = \sum_{i=0}^{n-1} \Delta_{\lambda_i}^{\lambda_{i+1}} G = -kT \sum_{i=0}^{n-1} \ln \left\langle \exp\left(-\frac{U(\lambda_{i+1}) - U(\lambda_i)}{kT} \right) \right\rangle_{\lambda_i} \quad (2)$$

In this study, λ = 0.01 was used and the interaction were modified in 100 stages (windows) over 100 ps NPT per window for the bulk (3D) system. Notably, the AMOEBA forcefield is rather complex and required us to extend LAMMPS to facilitate applying λ to vary the carbonate – water buffered 14-7 van der Waals interactions, the electronic polarization between induced point dipoles and the electrostatics between permanent point charges, dipoles, and quadrupoles. Our implementation was based on that of the Tinker MD Code.[29]

B.4. Accelerated Metadynamics simulations: We performed classical free energy sampling on equilibrated MD cells to evaluate the free energy profiles along the following collective variables (CVs): 1) The coordination number (CN) of carbonate ions to a central, randomly selected carbonate, and 2) the carbonate distance in the water slab. Specifically, we use the Metadynamics protocol to evaluate the potential of mean force along the collective variables.[30] The simulations were carried out using the Colvars[31] module in LAMMPS.

We use the following definition of CN:

$$\sum_{i=1}^{N} \frac{1-\left(\frac{r_i}{r_0}\right)^p}{1-\left(\frac{r_i}{r_0}\right)^q} \qquad (3)$$

where p=6, q=12, r_i is the distance between the center of mass of selected carbonate ion and the center of the water slab and r_0 = 8Å is the cut-off radius, chosen so that the maximum coordination number for our typical simulation cell (with 7 carbonates) was 6. MD simulation boxes (**Table S2**) after equilibration were used as initial configuration for the free energy sampling with the Metadynamics protocol. In the distance colvar, the z-coordinate of the selected carbonate, reference to the center of mass of the water slab (determined at the start of the Metadynamics simulation from the equilibrated structure and fixed) was used.

To facilitate efficient exploration of the rugged potential energy surface, we employed two recent advances in order to accelerate convergence: a) we used the well-tempered formulation,[32] where the bias deposition rate decreases over time by rescaling the heights of the deposited Gaussian functions; and b) we used the multiple walker scheme[33] with well-tempered simulations (MW-wt-MetaD). The parameters of the MW-wt-MetaD free energy sampling were thus: 35 walkers, selected to span all 7 coordination numbers and

5 distances from the center of the water slab of a randomly selected carbonate molecule in a simulation with 7 carbonates, height of the Gaussian hills = 1.2 kcal/mol, frequency of hill creation 1000 steps (1 ps), width of hills = 0.2 in Å for distance or unitless 0.02 for CN and total simulation time > 1 ms, with a well-tempered bias of 10x the simulation temperature. The converged 2D free energy profiles were plotted in Gnuplot v 5.4 Patchlevel 2.

Typically, free energy sampling was determined to be converged when both of the following conditions were met: 1) The phase space of interest for the simulation was entirely explored (i.e., all relevant carbonate distances in the solvent slab were visible in the profile), and 2) the standard deviation of free energy profiles converge to < 0.5 kcal/mol within the phase space of interest over the averaged time period (last 100 ns). For the carbonate systems, we found that the different sizes of ion aggregates across systems significantly affected the ability of the systems to reach ballistic motion along their respective CVs, which is responsible for criteria # 2. We monitored convergence by calculating the free energy profiles every 10ns and found that ~ 500ns was reasonable in most cases.

B.5. XPS binding energy simulation

Due to the relatively large size of the system, we performed another set of MD simulations on a smaller system of 15Å x 15Å x 60Å to generate snapshots for electronic structure calculations. Each representative structure has the targeted carbon-containing chemical species at the air-water interface and in the bulk. We employed ARES package to simulate XPS binding energy shifts of each C atom in the system.[34] ARES is a real-space pseudopotential electronic calculation package based on density functional theory, (DFT) with highly parallelizable features making the simulation of our system possible. For each system, 9 snapshots at the air/water interface from molecular dynamics simulation were taken as an input structure for binding energy calculations. The binding energies are

obtained by the total energy difference between the initial ground state and final excited state by using ΔSCF within density functional theory:

$$E_b = E^{N-1}\left[n_F\right] - E^N\left[n_I\right] \qquad (7)$$

Where $E^{N-1}[n_F]$ and $E^N[n_I]$ are the total energy functionals of the final and initial electron densities, respectively. Two PPs for carbon atoms with pseudo core and core-hole respectively are generated using the FHI98PP code[35] for the initial and final state calculations, respectively.[36] Under the fully-screened core-hole assumption, only the traditional self-consistent field (SCF) iterations are required for initial and final state calculations. In our calculations, a grid spacing of 0.15 Å was adopted to achieve well-converged total energies (within 1 meV/atom). The total energy convergence criterion of SCF iteration is within 0.1 meV.

To enable large-scale calculations with high accuracy, we carried out the calculations using one of our critical innovations regarding hybrid functionals.[36]. The SCF calculation is performed using PBE functional,[37] and then the refined step is introduced by an additional non-SCF calculation using the hybrid exchange-correlation functional (B3LYP),[38], which can robustly improve the accuracy of total energy and binding energy shifts at a low computational cost.[36] We included both results in **Figure S4** below. Compared to the result calculated by PBE functional in **Fig. S4a**, the average binding energy shift refined by B3LYP in **Fig. 4b** better agrees with the experiment by ~0.2 eV.

C. Supporting Tables

Table S1: Fitting Parameters from Langmuir Model of Adsorption for the carbonate anion, in *pp* and *sp* polarization schemes.

Anion	$\Delta G\left(\frac{kJ}{mol}\right)$	A	B	C
$CO_3^{2-}(pp)$	-11.1 $\pm$ 0.7	1.00	0.164	1.12
$CO_3^{2-}(sp)$	-11.1 $\pm$ 0.7	1.00	0.19	1.23
$CO_3^{2-}(pp)$	-2 **	0.99	3.5	-3.5×10^{-5}
$CO_3^{2-}(pp)$	+2**	0.99	17.2	4.2×10^{-4}

** indicates that the Gibb's free energy of adsorption was constrained during the fit, and parameters *A*, *B*, *C* were simultaneously solved for.

Table S2: Description of computational systems. Equilibration simulations were performed to calculate the carbonate structural properties as well as the water shell thermodynamics. Slab Metadynamics simulations were performed to determine the free energy surface. All slab simulations used a 1.9x1.9x9.0 nm^3 unit cell.

System	# carbonates	#Na^+	#water	Simulation time (equil/Metad) (ns)
Na_2CO_3 (bulk)	1 – 12 CO_3^{2-}	2 – 24	903	30
Na_2CO_3 (slab)	7 CO_3^{2-}	14	646	30/1050
$NaHCO_3$ (bulk)	1 – 12 HCO_3^-	1 – 12	903	30
$NaHCO_3$ (slab)	7 HCO_3^-	7	646	30/700
H_2CO_3 (bulk)	7 H_2CO_3	0	900	30
H_2CO_3 (slab)	7 $H_2CO_3^-$	0	646	30/350
CO_2 (bulk)	7 CO_2	0	900	30
CO_3 (slab)	7 CO_2	0	646	30/175

Table S3: Hydration free energy (ΔG_{hyd} kJ/mol) of various carbonate species, described using the AMOEBA forcefield. Free energy perturbation (FEP) calculations are performed using the TINKER code.[39] Reference hydration energies from experiments, previous FEP calculations, QM calculations (this work), are provided as available.

System	#Na^+	#water	ΔG_{hyd}(FEP)	Reference
H_2O	0	333	-24.0 ± 1.2	Calc: -23.6 (FEP)[2] Exp: -26.4[40]
CO_3^{2-}	2	333	-1317.7 ± 5.5	Calc: -1314±3 (FEP)[2], -1204.3 (QM) Exp: -1315[41], -1324[42]
HCO_3^-	1	333	-338.1 ± 5.3	Calc: -346±1 (FEP)[2] -370.4 (QM) Exp: -335[41],-343[42],-368[43]
H_2CO_3	0	333	-108.1 ± 5.2	Calc: -117 (QM)
CO_2	0	333	4.5 ± 0.5	Calc: 4.4[44] Exp: 1.0[45]

Table S4: Structural properties of solid carbonates. Equivalent orthogonal cells were created using the Atomsk toolkit,[46] and cell relaxation calculations performed using LAMMPS.

Solid	Primitive cell	(Orthorhombic) supercell	Optimized supercell	% Δvol
Natrite (Na_2CO_3) ICSD Collection code: 168128	a= 8.825 Å b= 5.194 Å c= 5.953 Å α = γ = 90° β = 101.83°	a= 17.65 Å b= 10.388 Å c= 168.97 Å	a= 17.88 Å b= 10.50 Å c= 171.40 Å	+3.9
Thermonatrite ($NaCO_3 \cdot H_2O$) ICSD Collection code: 1852	a= 6.472 Å b= 10.724 Å c= 5.259 Å α = β = γ = 90°	a= 12.944 Å b= 10.724 Å c= 10.518 Å	a= 12.934 Å b= 10.719 Å c= 10.529 Å	-0.02
Sodium hydrogencarbonate ($NaHCO_3$) ICSD Collection code: 18183	a= 3.51 Å b= 9.71 Å c= 8.05 Å α = γ = 90° β = 111.85°	a= 10.53 Å b= 19.42 Å c= 52.302 Å	a= 10.75 Å b= 19.58 Å c= 53.81 Å	+5.92
Carbon dioxide (CO_2 – 1 GPa) ICSD Collection code: 59378	a= b= c= 5.4942Å α = β = γ = 90°	a= b = c = 10.988Å	a= 11.2642 Å b= 11.2643 Å	+7.73

			c= 11.2642 Å	

D. Supporting Figures

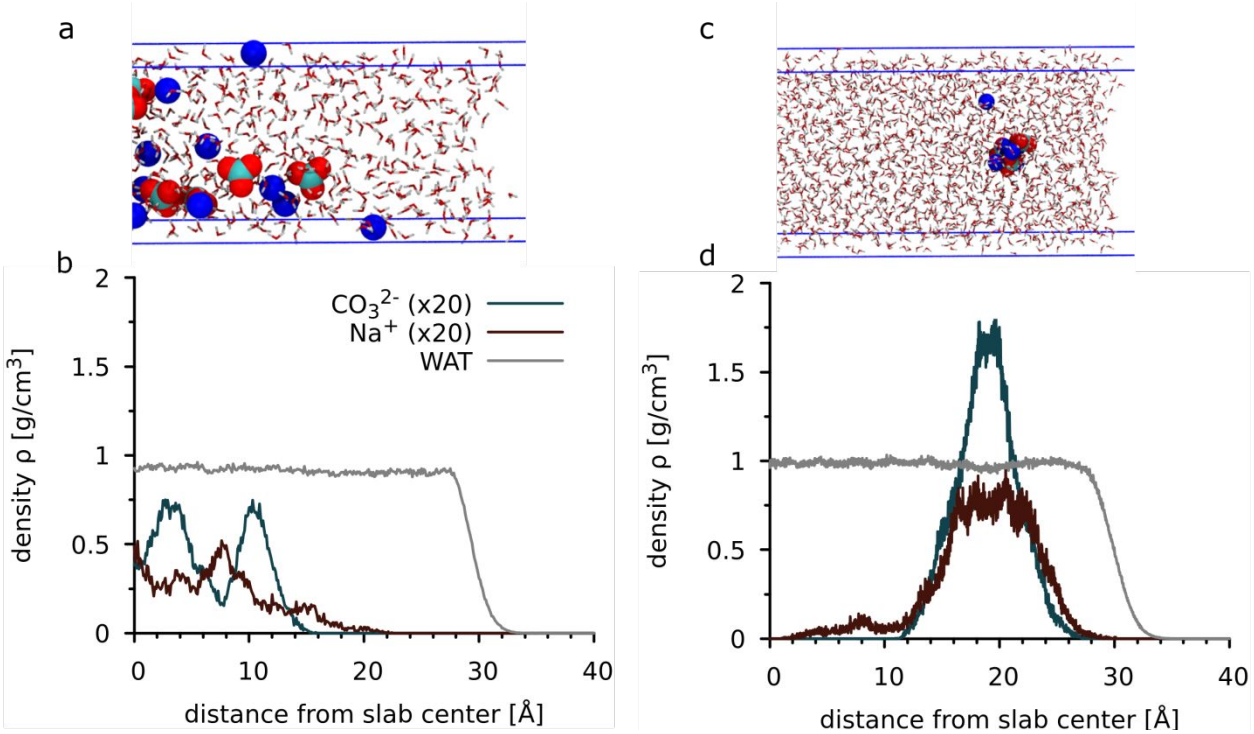

Figure S1: Structure and density of carbonate systems. **a**) Snapshot of the equilibrium structure of 1.0 M Na_2CO_3 (15 molecule) solution near the air/water interface. The simulation was initiated from a random distribution of ions in the water slab. The sodium and carbonate ions are shown in the blue and red/green spheres, respectively. **b**) Corresponding density profile of the carbonate anion (green line), sodium cation (red line) and water (grey line), as a function of distance from the slab center. Note that the density of the ions is scaled by a factor of 20 for visualization purposes. **c**) Snapshot of the equilibrium structure of 0.2M Na2CO3 solution near the air/water interface. Here the simulation was initiated by placing an energy minimized, 3-molecule cluster near the interface, which persisted on the timescale of our 20nm MD simulation. **d**) Density profile of the 0.2M Na_2CO_3 solution.

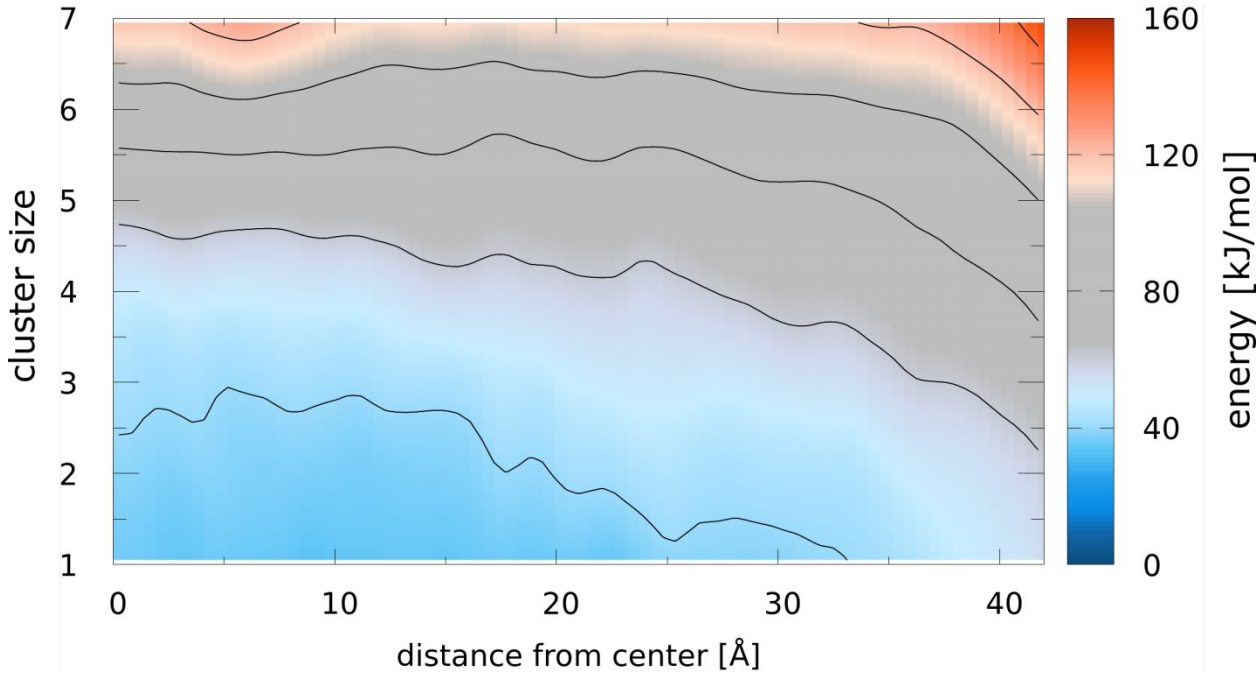

Figure S2: 2D FES of carbonic acid (H_2CO_3) from accelerated Metadynamics MD simulations.

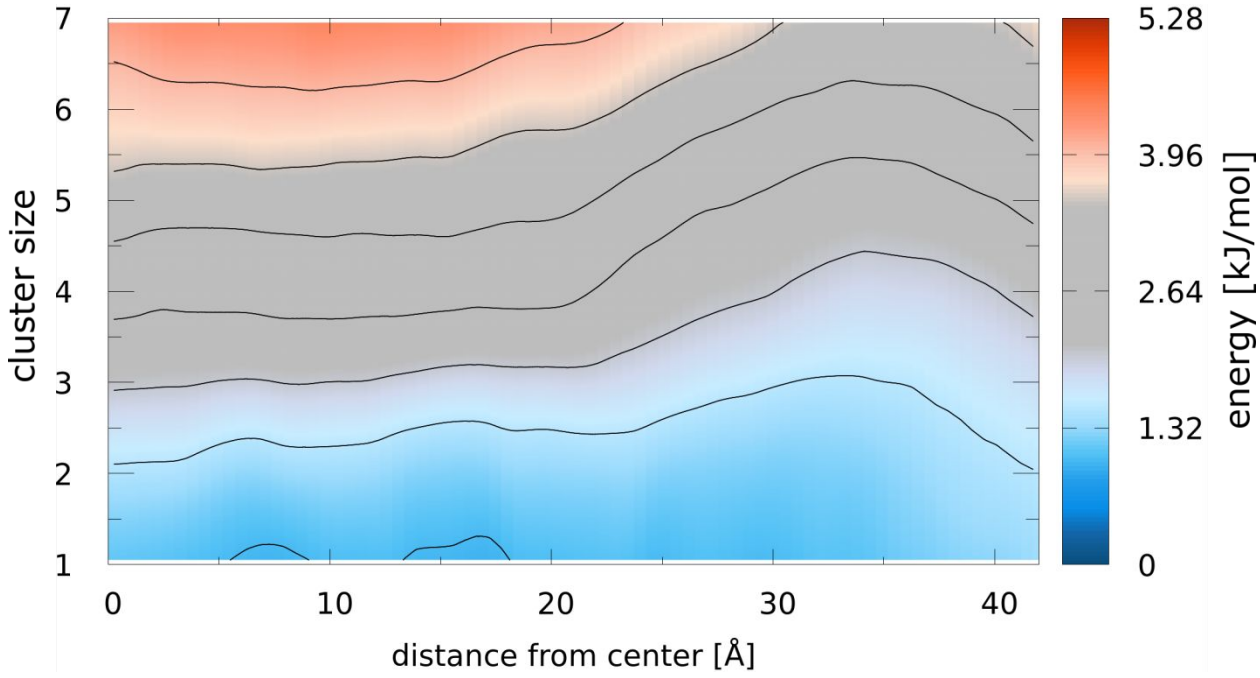

Figure S3: 2D FES of Carbon dioxide (CO_2)

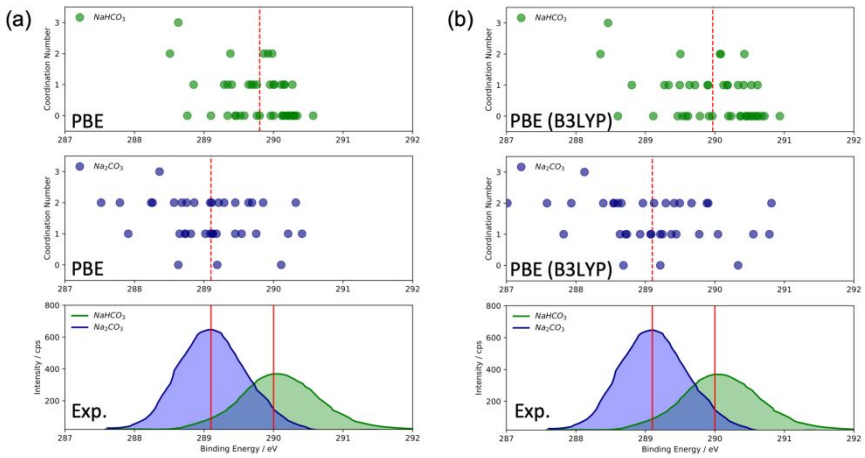

Figure S4. The binding energies for C (1s) excitation were calculated by density functional theory using (a) PBE functional and (b) PBE-based SCF calculations refined by B3LYP.

E. Carbonates AMOEBA Forcefield

!! DATE: 2023-06-05 UNITS: real

```
    ################################
    ##                            ##
    ##  Force Field Definition    ##
    ##                            ##
    ################################


forcefield              CARBONATES-2023

bond-cubic              -2.55
bond-quartic             3.793125
angle-cubic             -0.014
angle-quartic            0.000056
angle-pentic            -0.0000007
angle-sextic            0.000000022
opbendtype               ALLINGER
opbend-cubic            -0.014
opbend-quartic           0.000056
opbend-pentic           -0.0000007
opbend-sextic           0.000000022
torsionunit             0.5
vdwtype                 BUFFERED-14-7
```

```
radiusrule            CUBIC-MEAN
radiustype            R-MIN
radiussize            DIAMETER
epsilonrule           HHG
dielectric            1.0
polarization          MUTUAL
vdw-12-scale          0.0
vdw-13-scale          0.0
vdw-14-scale          1.0
vdw-15-scale          1.0
mpole-12-scale        0.0
mpole-13-scale        0.0
mpole-14-scale        0.4
#mpole-15-scale        0.8
polar-12-scale        0.0
polar-13-scale        0.0
polar-14-scale        1.0
polar-15-scale        1.0
polar-12-intra        0.0
polar-13-intra        0.0
polar-14-intra        0.5
polar-15-intra        1.0
direct-11-scale       0.0
direct-12-scale       1.0
direct-13-scale       1.0
direct-14-scale       1.0
mutual-11-scale       1.0
mutual-12-scale       1.0
mutual-13-scale       1.0
mutual-14-scale       1.0


  ################################
  ##                            ##
  ##  Literature References     ##
  ##                            ##
  ################################
```

Walker, B., Liu, C., Wait, E., Ren, P., J. Comput. Chem. 2022, 1. https://doi.org/10.1002/jcc.26954
Wu, J.C.; Chattree, G.; Ren, P.Y.; Automation of AMOEBA polarizable force field parameterization for small molecules. Theor Chem Acc.

```
  ##############################
  ##                          ##
  ##  Atom Type Definitions   ##
  ##                          ##
  ##############################


atom        1    1   OW    "AMOEBA Water O         "        8    15.995    2
atom        2    2   HW    "AMOEBA Water H         "        1     1.008    1
atom        3    3   C_HC  "Bicarbonate C           "        6    12.011    3
atom        4    4   O_2HC "Bicarbonate O          "        8    15.999    1
atom        5    5   O_3HC "Bicarbonate O(H)       "        8    15.999    2
atom        6    6   H_HC  "Bicarbonate H          "        1     1.008    1
atom        7    7   C_CA  "C in Carbonic Acid      "        6    12.011    3
atom        8    8   O_2CA "O in Carbonic Acid      "        8    15.999    1
atom        9    9   O_3CA "O(H) in Carbonic Acid   "        8    15.999    2
atom       10   10   H_CA  "H in Carbonic Acid      "        1     1.008    1
atom       11   11   C_OCA "H in Orthocarbonic acid "        6    12.011    4
atom       12   12   O_OCA "O in Orthocarbonic acid "        8    15.999    2
atom       13   13   H_OCA "H in Orthocarbonic acid "        1     1.008    1
atom       14   14   C_C   "Carbonate C            "        6    12.011    3
atom       15   15   O_2C  "Carbonate O            "        8    15.999    1
atom       16   16   Na+   "Sodium Ion Na+         "       11    22.990    0
atom       17   17   Cl-   "Chloride Ion Cl-       "       17    35.453    0
atom       18   18   C_11  "C in Carbon Dixoide    "        6    12.011    2
atom       19   19   O_21  "O in Carbon Dixoide    "        8    15.999    1


  ##################################
  ##                              ##
  ##  Van der Waals Parameters    ##
  ##                              ##
  ##################################


vdw         1          3.4050    0.1100
vdw         2          2.6550    0.0135    0.9100
vdw         3          3.6700    0.1060
vdw         4          3.6800    0.0950
vdw         5          3.6800    0.0950
vdw         6          2.2550    0.0150    0.9100
vdw         7          3.6700    0.1060
vdw         8          3.6800    0.0950
```

```
vdw         9           3.6800    0.0950
vdw        10           2.2550    0.0150    0.9100
vdw        11           3.6700    0.1060
vdw        12           3.6800    0.0950
vdw        13           2.2550    0.0150    0.9100
vdw        14           3.6500    0.1060
vdw        15           3.5950    0.1050
vdw        16           2.9550    0.2800
vdw        17           4.1200    0.3400
vdw        18           3.6700    0.1060
vdw        19           3.6800    0.0950


  ####################################
  ##                                ##
  ##  Bond Stretching Parameters    ##
  ##                                ##
  ####################################


bond        1    2    556.85    0.9572
bond        4    3    605.00    1.2525
bond        5    3    331.60    1.4540
bond        6    5    514.40    0.9737
bond        7    8    605.00    1.2525
bond        7    9    331.60    1.4540
bond       10    9    514.40    0.9737
bond       12   11    214.78    1.3900
bond       13   12    497.05    0.9700
bond       14   15    505.00    1.3100
bond       18   19    465.00    1.1800


  ###################################
  ##                               ##
  ##  Angle Bending Parameters     ##
  ##                               ##
  ###################################


angle       2    1    2     48.70   108.5000
angle       4    3    4    102.50   133.0400
angle       5    3    4     92.30   113.4800
angle       6    5    3     49.60   108.7000
```

```
angle        7    9   10     49.60   108.7000
angle        8    7    9     92.30   113.4800
angle        9    7    9    102.50   133.0400
angle       12   11   12     65.00   109.4700
angle       13   12   11     32.14    98.7067
angle       15   14   15    120.00   120.0000
angle       19   18   19     65.00   180.0000

   ################################
   ##                            ##
   ##  Urey-Bradley Parameters   ##
   ##                            ##
   ################################

ureybrad     2    1    2     -7.60     1.5537

  ################################
  ##                            ##
  ##  Stretch-Bend Parameters   ##
  ##                            ##
  ################################


strbnd       4    3    4     18.70    18.7000
strbnd       5    3    4     18.70    18.7000
strbnd       8    7    9     18.70    18.7000
strbnd       9    7    9     18.70    18.7000
strbnd      12   11   12     18.70    18.7000
strbnd      13   12   11     18.70    18.7000
strbnd      15   14   15     18.70    18.7000
strbnd      19   18   19     18.70    18.7000


  ####################################
  ##                                ##
  ##  Out-of-Plane Bend Parameters  ##
  ##                                ##
  ####################################


opbend       4    3    5    4    242.00
opbend       8    7    9    9    242.00
opbend      15   14   15   15    242.00
```

```
  ##############################
  ##                          ##
  ##  Torsional Parameters    ##
  ##                          ##
  ##############################


torsion   6  5  3   4 -1.051   0.0  1 10.091 180.0  2 -1.054   0.0  3 0.129 180.0  4 -1.052   0.0  5
0.004 180.0  6
torsion   10 9  7   8 -5.867   0.0  1 4.857  180.0  2  2.911   0.0  3 0.562 180.0  4  2.499   0.0  5
0.377 180.0  6
torsion   10 9  7   9  2.417   0.0  1 4.859  180.0  2  1.415   0.0  3 0.562 180.0  4  2.103   0.0  5
0.377 180.0  6
torsion   13 12 11 12  2.417   0.0  1 4.859  180.0  2  1.415   0.0  3 0.562 180.0  4  2.103   0.0  5
0.377 180.0  6


  ####################################
  ##                                ##
  ##  Atomic Multipole Parameters   ##
  ##                                ##
  ####################################


multipole     1   -2   -2          -0.51966
                        0.00000   0.00000   0.14279
                        0.37928
                        0.00000  -0.41809
                        0.00000   0.00000   0.03881

multipole     2    1    2           0.25983
                       -0.03859   0.00000  -0.05818
                       -0.03673
                        0.00000  -0.10739
                       -0.00203   0.00000   0.14412

multipole     3   -4   -4           1.24761
                       -0.02780   0.00000  -0.12783
                        0.04256
                        0.00000  -0.18474
                        0.06473   0.00000   0.14218

multipole     4    3    5          -0.92733
```

-0.04328 0.00000 -0.05066
-0.30699
0.00000 0.01888
-0.03525 0.00000 0.28811

multipole 5 6 3 -0.62219
0.23755 0.00000 -0.04595
0.61449
0.00000 -0.46373
-0.29267 0.00000 -0.15076

multipole 6 5 3 0.22924
0.00476 0.00000 -0.08657
0.00000
0.00000 0.00000
0.00000 0.00000 0.00000

multipole 7 -9 -9 0.97226
0.00000 0.00000 0.02861
0.11412
0.00000 -0.24518
0.00000 0.00000 0.13106

multipole 8 7 -0.66458
0.00000 0.00000 -0.12738
-0.08161
0.00000 -0.08161
0.00000 0.00000 0.16322

multipole 9 10 7 -0.40978
0.08061 0.00000 0.20129
0.00177
0.00000 -0.41250
-0.08714 0.00000 0.41073

multipole 10 9 7 0.25594
-0.07352 0.00000 -0.03684
-0.04467
0.00000 -0.09356
0.05090 0.00000 0.13823

multipole 11 12 1.15952
0.00000 0.00000 0.00000
0.00042

```
                    0.00000   0.00042
                    0.00000   0.00000  -0.00084

multipole    12   13   11          -0.52987
                    0.07322   0.00000   0.18221
                    0.12930
                    0.00000  -0.55455
                   -0.14635   0.00000   0.42525

multipole    13   12   11           0.23999
                   -0.06627   0.00000  -0.01124
                   -0.08946
                    0.00000  -0.10662
                    0.05040   0.00000   0.19608

multipole    14   15               1.31911
                    0.00000   0.00000   0.00000
                    0.02323
                    0.00000  -0.04646
                    0.00000   0.00000   0.02323

multipole    15   14              -1.10637
                    0.00000   0.00000   0.13933
                   -0.47678
                    0.00000  -0.28195
                    0.00000   0.00000   0.75873

multipole    16    0    0           1.00000
                    0.00000   0.00000   0.00000
                    0.00000
                    0.00000   0.00000
                    0.00000   0.00000   0.00000

multipole    17    0    0          -1.00000
                    0.00000   0.00000   0.00000
                    0.00000
                    0.00000   0.00000
                    0.00000   0.00000   0.00000

multipole    18                    0.82798
                    0.00000   0.00000   0.00000
                    0.00000
                    0.00000   0.00000
                    0.00000   0.00000   0.00000
```

```
multipole    19    18               -0.41399
                        0.00000   0.00000  -0.09772
                       -0.00417
                        0.00000  -0.00417
                        0.00000   0.00000   0.00834


  ########################################
  ##                                    ##
  ##  Dipole Polarizability Parameters  ##
  ##                                    ##
  ########################################


polarize      1          0.8370    0.3900    2
polarize      2          0.4960    0.3900    1
polarize      3          1.3340    0.3900    4    5
polarize      4          0.8370    0.3900    3
polarize      5          0.8370    0.3900    3    6
polarize      6          0.4960    0.3900    5
polarize      7          1.3340    0.3900    8    9
polarize      8          0.8370    0.3900    7
polarize      9          0.8370    0.3900    7   10
polarize     10          0.4960    0.3900    9
polarize     11          1.3340    0.3900   12
polarize     12          0.8370    0.3900   11   13
polarize     13          0.4960    0.3900   12
polarize     14          1.3340    0.3900   15
polarize     15          0.8370    0.3900   14
polarize     16          0.1200    0.3900
polarize     17          4.0000    0.3900
polarize     18          1.3340    0.3900   19
polarize     19          0.8370    0.3900   18
```

F. Supporting References

1. Petersen, P. B.; Saykally, R. J., Probing the interfacial structure of aqueous electrolytes with femtosecond second harmonic generation spectroscopy. ACS Publications: 2006; Vol. 110, pp 14060-14073.
2. Raiteri, P.; Schuitemaker, A.; Gale, J. D., Ion pairing and multiple ion binding in calcium carbonate solutions based on a polarizable AMOEBA force field and ab initio molecular dynamics. *J. Phys. Chem. B* **2020,** *124* (17), 3568-3582.

3. Byrne, E. H.; Raiteri, P.; Gale, J. D., Computational Insight into Calcium–Sulfate Ion Pair Formation. *J. Phys. Chem. C* **2017,** *121* (46), 25956-25966.
4. Huang, Y. C.; Rao, A.; Huang, S. J.; Chang, C. Y.; Drechsler, M.; Knaus, J.; Chan, J. C. C.; Raiteri, P.; Gale, J. D.; Gebauer, D., Uncovering the Role of Bicarbonate in Calcium Carbonate Formation at Near-Neutral pH. *Angewandte Chemie International Edition* **2021,** *60* (30), 16707-16713.
5. Ponder, J. W.; Wu, C.; Ren, P.; Pande, V. S.; Chodera, J. D.; Schnieders, M. J.; Haque, I.; Mobley, D. L.; Lambrecht, D. S.; DiStasio, R. A.; Head-Gordon, M.; Clark, G. N. I.; Johnson, M. E.; Head-Gordon, T., Current Status of the AMOEBA Polarizable Force Field. *J. Phys. Chem. B* **2010,** *114* (8), 2549-2564.
6. Walker, B.; Liu, C.; Wait, E.; Ren, P., Automation of AMOEBA polarizable force field for small molecules: Poltype 2. *J Comput Chem* **2022,** *43* (23), 1530-1542.
7. Cramer, C. J.; Truhlar, D. G., A universal approach to solvation modeling. *Accounts of chemical research* **2008,** *41* (6), 760-768.
8. Shao, Y.; Gan, Z.; Epifanovsky, E.; Gilbert, A. T.; Wormit, M.; Kussmann, J.; Lange, A. W.; Behn, A.; Deng, J.; Feng, X., Advances in molecular quantum chemistry contained in the Q-Chem 4 program package. *Mol Phys* **2015,** *113* (2), 184-215.
9. Thompson, A. P.; Aktulga, H. M.; Berger, R.; Bolintineanu, D. S.; Brown, W. M.; Crozier, P. S.; in't Veld, P. J.; Kohlmeyer, A.; Moore, S. G.; Nguyen, T. D., LAMMPS-a flexible simulation tool for particle-based materials modeling at the atomic, meso, and continuum scales. *Comput Phys Commun* **2022,** *271*, 108171.
10. Pascal, T. A.; Schwartz, C. P.; Lawler, K. V.; Prendergast, D., The purported square ice in bilayer graphene is a nanoscale, monolayer object. *J. Chem. Phys.* **2019,** *150* (23), 231101.
11. Shrestha, B. R.; Pillai, S.; Santana, A.; Donaldson Jr, S. H.; Pascal, T. A.; Mishra, H., Nuclear Quantum Effects in Hydrophobic Nanoconfinement. *J. Phys. Chem. Lett.* **2019,** *10* (18), 5530-5535.
12. Pascal, T. A.; Villaluenga, I.; Wujcik, K. H.; Devaux, D.; Jiang, X.; Wang, D. R.; Balsara, N.; Prendergast, D., Liquid Sulfur Impregnation of Microporous Carbon Accelerated by Nanoscale Interfacial Effects. *Nano Lett.* **2017,** *17* (4), 2517-2523.
13. Li, C.; Ward, A. L.; Doris, S. E.; Pascal, T. A.; Prendergast, D.; Helms, B. A., Polysulfide-Blocking Microporous Polymer Membrane Tailored for Hybrid Li-Sulfur Flow Batteries. *Nano Lett.* **2015,** *15* (9), 5724-5729.
14. Pascal, T. A.; Goddard III, W. A., Interfacial Thermodynamics of Water and Six Other Liquid Solvents. *J. Phys. Chem. B* **2014,** *118* (22), 5943-5956.
15. Jeon, J.; Kim, H.; Goddard III, W. A.; Pascal, T. A.; Lee, G.-I.; Kang, J. K., The role of confined water in ionic liquid electrolytes for dye-sensitized solar cells. *J. Phys. Chem. Lett.* **2012,** *3* (4), 556-559.
16. Pascal, T. A.; Goddard III, W. A.; Maiti, P. K.; Vaidehi, N., Role of specific cations and water entropy on the stability of branched DNA motif structures. *J. Phys. Chem. B* **2012,** *116* (40), 12159-12167.
17. Pascal, T. A.; Goddard III, W. A., Hydrophobic Segregation, Phase Transitions and the Anomalous Thermodynamics of Water/Methanol Mixtures. *J. Phys. Chem. B* **2012,** *116* (47), 13905-13912.

18. Pascal, T. A.; Schärf, D.; Jung, Y.; Kühne, T. D., On the absolute thermodynamics of water from computer simulations: A comparison of first-principles molecular dynamics, reactive and empirical force fields. *J. Chem. Phys.* **2012,** *137* (24), 244507.
19. Pascal, T. A.; Goddard, W. A.; Jung, Y., Entropy and the driving force for the filling of carbon nanotubes with water. *Proc. Natl. Acad. Sci. U. S. A.* **2011,** *108* (29), 11794-11798.
20. Pascal, T. A.; Lin, S.-T.; Goddard III, W. A., Thermodynamics of liquids: standard molar entropies and heat capacities of common solvents from 2PT molecular dynamics. *Phys. Chem. Chem. Phys.* **2011,** *13* (1), 169-181.
21. Pascal, T. A.; He, Y.; Jiang, S.; Goddard III, W. A., Thermodynamics of Water Stabilization of Carboxybetaine Hydrogels from Molecular Dynamics Simulations. *J. Phys. Chem. Lett.* **2011,** *2* (14), 1757-1760.
22. Pascal, T. A.; Abrol, R.; Mittal, R.; Wang, Y.; Prasadarao, N. V.; Goddard, W. A., Experimental Validation of the Predicted Binding Site of Escherichia coli K1 Outer Membrane Protein A to Human Brain Microvascular Endothelial Cells IDENTIFICATION OF CRITICAL MUTATIONS THAT PREVENT E. COLI MENINGITIS. *Journal of Biological Chemistry* **2010,** *285* (48), 37753-37761.
23. Shinoda, W.; Shiga, M.; Mikami, M., Rapid estimation of elastic constants by molecular dynamics simulation under constant stress. *Physical Review B* **2004,** *69* (13), 134103.
24. Martyna, G. J.; Tobias, D. J.; Klein, M. L., Constant pressure molecular dynamics algorithms. *J. Chem. Phys.* **1994,** *101* (5), 4177-4189.
25. Parrinello, M.; Rahman, A., Polymorphic transitions in single crystals: A new molecular dynamics method. *J. Appl. Phys.* **1981,** *52* (12), 7182-7190.
26. Tuckerman, M. E.; Alejandre, J.; López-Rendón, R.; Jochim, A. L.; Martyna, G. J., A Liouville-operator derived measure-preserving integrator for molecular dynamics simulations in the isothermal–isobaric ensemble. *J. Phys. A: Math. Gen.* **2006,** *39* (19), 5629.
27. Zwanzig, R. W., High-Temperature Equation of State by a Perturbation Method. I. Nonpolar Gases. *The Journal of Chemical Physics* **1954,** *22*, 1420.
28. Liu, H.; Holoubek, J.; Zhou, H.; Chen, A.; Chang, N.; Wu, Z.; Yu, S.; Yan, Q.; Xing, X.; Li, Y.; Pascal, T. A.; Liu, P., Ultrahigh coulombic efficiency electrolyte enables Li||SPAN batteries with superior cycling performance. *Materials Today* **2021,** *42*, 17-28.
29. https://dasher.wustl.edu/tinker/
30. Barducci, A.; Bonomi, M.; Parrinello, M., Metadynamics. *WIREs Computational Molecular Science* **2011,** *1* (5), 826-843.
31. Fiorin, G.; Klein, M. L.; Hénin, J., Using collective variables to drive molecular dynamics simulations. *Mol Phys* **2013,** *111* (22-23), 3345-3362.
32. Barducci, A.; Bussi, G.; Parrinello, M., Well-tempered metadynamics: a smoothly converging and tunable free-energy method. *Phys. Rev. Lett.* **2008,** *100* (2), 020603.
33. Raiteri, P.; Laio, A.; Gervasio, F. L.; Micheletti, C.; Parrinello, M., Efficient reconstruction of complex free energy landscapes by multiple walkers metadynamics. *J. Phys. Chem. B* **2006,** *110* (8), 3533-3539.
34. Xu, Q.; Wang, S.; Xue, L.; Shao, X.; Gao, P.; Lv, J.; Wang, Y.; Ma, Y., Ab initio electronic structure calculations using a real-space Chebyshev-filtered subspace iteration method. *J. Phys.: Condens. Matter* **2019,** *31* (45), 455901.

35. Fuchs, M.; Scheffler, M., Ab initio pseudopotentials for electronic structure calculations of poly-atomic systems using density-functional theory. *Comput Phys Commun* **1999,** *119* (1), 67-98.
36. Xu, Q.; Prendergast, D.; Qian, J., Real-Space pseudopotential method for the calculation of 1 s core-level binding energies. *Journal of chemical theory and computation* **2022,** *18* (9), 5471-5478.
37. Perdew, J. P.; Burke, K.; Ernzerhof, M., Generalized gradient approximation made simple. *Phys. Rev. Lett.* **1996,** *77* (18), 3865-3868.
38. Becke, A. D., Density-functional thermochemistry. III. The role of exact exchange. *J. Chem. Phys.* **1993,** *98* (7), 5648-5652.
39. Rackers, J. A.; Wang, Z.; Lu, C.; Laury, M. L.; Lagardère, L.; Schnieders, M. J.; Piquemal, J.-P.; Ren, P.; Ponder, J. W., Tinker 8: software tools for molecular design. *Journal of chemical theory and computation* **2018,** *14* (10), 5273-5289.
40. Ben-Naim, A.; Marcus, Y., Solvation thermodynamics of nonionic solutes. *J. Chem. Phys.* **1984,** *81* (4), 2016-2027.
41. Marcus, Y., *Ions in Solution and their Solvation*. John Wiley & Sons: 2015.
42. Marcus, Y., *Ion solvation*. Wiley: 1985.
43. Marcus, Y., A simple empirical model describing the thermodynamics of hydration of ions of widely varying charges, sizes, and shapes. *Biophysical chemistry* **1994,** *51* (2-3), 111-127.
44. Jiao, D.; Rempe, S. B., CO2 solvation free energy using quasi-chemical theory. *J. Chem. Phys.* **2011,** *134* (22).
45. Lide, D. R., *CRC handbook of chemistry and physics*. CRC press: 2004; Vol. 85.
46. Hirel, P., Atomsk: A tool for manipulating and converting atomic data files. *Comput Phys Commun* **2015,** *197*, 212-219.